Journal of the Ceramic Society of Japan 121 [8] 706-709 2013 Paper

High-temperature thermoelectric properties of $BaFe_xTi_{1-x}O_{3-\delta}$ ceramics

Tomofumi YAMADA, Rintaro AOYAGI,† Takeshi YOKOTA and Manabu GOMI

Graduate School of Engineering, Nagoya Institute of Technology, Gokiso-cho, Showa-ku, Nagoya 466–8555, Japan

High-temperature thermoelectric properties of $BaFe_xTi_{1-x}O_{3-\delta}$ (BFT100x) ceramics in air were investigated. Crystal structures of BFT100x ceramics were found to be a mixture of tetragonal or cubic provskite and hexagonal $BaTiO_3$ phases for $x = 0.05$–0.20, and a single phase of hexagonal $BaTiO_3$ for $x > 0.30$. X-ray diffraction pattern of BFT90 revealed a mixture of hexagonal $BaTiO_3$ and monoclinic $Ba_2Fe_2O_5$ phases. Conductivity of BFT100x increased with increase in temperature and Fe concentration. This increase in conductivity originated from the substitution of Ti^{4+} with Fe^{3+}, which increased the oxygen vacancy of the system. A maximum conductivity of 3.1×10^2 S/m was obtained for BFT90 at 1100 K. Activation energy calculated by resistivity decreased with increase in Fe concentration. Seebeck coefficient of BFT100x increased with increase in temperature and decreased with increase in Fe concentration for $x = 0.40$–0.80. These results suggested an increase in carrier concentration. Seebeck coefficient of BFT90 was larger than that of BFT80, which is attributable to the mixed structure of BFT90. Power factor of BFT100x increased with increase in temperature and Fe concentration. These results suggested that $BaFe_xTi_{1-x}O_{3-\delta}$ with mixed structure of hexagonal and monoclinic phases have good potential for enhancing the thermoelectric properties of $BaFe_xTi_{1-x}O_{3-\delta}$ ceramics.

Key-words : Thermoelectric properties, Seebeck coefficient, $BaTiO_3$–$BaFeO_{3-\delta}$, Power factor, Oxygen vacancy

[Received April 1, 2013; Accepted June 4, 2013]

1. Introduction

Thermoelectric materials directly convert heat into electric energy and vice versa through thermoelectric phenomena in solids. This method of transforming heat into electricity is a viable one for generating clean energy. The energy conversion function of thermoelectric power generation is governed by the dimensionless figure of merit

$$ZT = S^2\sigma T/\kappa, \quad (1)$$

where T is absolute temperature, S is thermoelectric power, σ is electrical conductivity, and κ is thermal conductivity. Therefore, a high power factor ($S^2\sigma$) and a low thermal conductivity are prerequisites for thermoelectric materials and related devices.[1] Conventional thermoelectric materials such as Bi_2Te_3,[2)–4)] Pb_2Te_3,[5)] Si–Ge alloys,[6)–8)] β-$FeSi_2$,[9)] and SiC[10),11)] have large thermoelectric power, but the thermal and chemical stability of Bi_2Te_3 and Pb_2Te_3 at high temperatures in air are unsatisfactory for thermoelectric conversion. Si–Ge alloy, β-$FeSi_2$, and SiC are stable at high temperature in air, however manufacturing cost of Si–Ge alloy and SiC are high, and thermal conductivity of β-$FeSi_2$ is large.

Oxide semiconductors are thermally and chemically stable in air and at high temperatures and can be easily manufactured at low cost. As a result, they have recently attracted attention as new high-temperature thermoelectric materials. Terasaki et al.[12)] found that $NaCo_2O_4$ single crystals exhibited good thermoelectric properties. Following a report on $NaCo_2O_4$,[13)] several thermoelectric oxide materials, such as $SrTiO_3$,[14)–16)] Li-doped NiO,[17)] $CaMnO_3$,[18),19)] and $Ca_3Co_4O_9$,[20)] have been reported. $NaCo_2O_4$ is susceptible to moisture in air and does not readily exhibit high thermoelectric properties in air. $SrTiO_3$ and Li-doped NiO exhibit n-type conductivity. Therefore, p-type thermoelectric oxide material using at high temperature is required.

Earlier studies[21)–29)] have reported the crystal structure and magnetic and electrical properties of $BaFe_xTi_{1-x}O_{3-\delta}$. Honbo et al. reported that $BaFeO_{3-\delta}$ showed hopping conductivity at high temperatures.[30)] Hopping conductivity is expected with a large Seebeck coefficient and conductivity. Maier and Cohn[24)] reported that resistivity of thin-film BFT100x decreased with increase in Fe concentration and temperature. Because of the hopping conductivity at high temperature, BFT100x is expected to be utilized as a high-temperature thermoelectric material. Therefore, in this study, we investigated the high-temperature thermoelectric properties of $BaFe_xTi_{1-x}O_{3-\delta}$ (BFT100x, $x =$ 0–0.9) bulk ceramics.

2. Experimental

Commercially available high-purity powders of $BaCO_3$ (Kojundo Chemical Lab., 99.9%), TiO_2 (Kojundo Chemical Lab., 99.9%), and Fe_2O_3 (Kojundo Chemical Lab., 99.9%) were employed as starting materials. After weighing, the powders were ball-milled with ethanol for 15 h. Next, the mixtures were dried and calcined in air at 1223 K for 10 h. After calcination, the powders were reground with ethanol in a ball mill for 20 h and pressed into pellets ($\phi 13 \times 3$ mm). Finally, these pellets were sintered in air at 1473 or 1573 K for 2 h. The crystal structure of the obtained sample was identified by powder X-ray diffraction (XRD) (Rigaku, RINT2100) using Cu Kα radiation. The pellets were cut into rectangles ($3 \times 3 \times 10$ mm) for electrical measurement. Resistivity ρ was measured by the two-probe method from room temperature to 500 K (ADCMT, 8340A), and the thermo-

† Corresponding author: R. Aoyagi; E-mail: aoyagi@nitech.ac.jp

DOI http://dx.doi.org/10.2109/jcersj2.121.706

electric properties were measured in air from 600 to 1200 K using a conductivity and Seebeck coefficient measurement system (Ozawa Science, RZ2001i).

3. Results and discussion

The sintering temperatures were fixed at 1573 or 1473 K. The samples with Fe-rich composition ($x = 0.80$ and 0.90) slightly melted after sintering at 1573 K. Therefore these compositions were sintered at 1473 K for 2 h. It was confirmed that the average grain size of sintered body increased with increase Fe concentration in same sintering temperature. The density of sintered samples was measured using Archimedes' Principle. The ratios of the measured density of the samples to the theoretical density are higher than 90%. The theoretical density of each composition was estimated by ICDD powder diffraction files, No. 05-0626 for tetragonal $BaTiO_3$ and No. 70-0034 for hexagonal $BaFeO_{2.73}$.

The XRD patterns of the $BaFe_xTi_{1-x}O_{3-\delta}$ powder are shown in **Fig. 1**. A pure $BaTiO_3$ tetragonal perovskite structure (*c*-BT) was obtained for $x = 0.00$. As the Fe concentration increases from 0.05 to 0.20, diffraction peaks belonging to a hexagonal BT structure (*h*-BT) were detected in addition to those of cubic or tetragonal perovskite BT structure (*c*-BT). Peak intensity of *h*-BT increased and that of *c*-BT decreased with increase in Fe concentration from 0.05 to 0.20. Earlier studies have reported that a pure hexagonal phase was detected for $x = 0.10$;[22),28)] however, a mixed structure of *h*-BT and *c*-BT was obtained for $x = 0.20$, as seen in Fig. 1. Figure 1 also reveals that a single phase of *h*-BT was observed for $x = 0.30$–0.80. Gerry et al.[22)] reported that the hexagonal phase of BFT100*x* was not stable at 1473 K for $x > 0.67$. Unlike their results, our samples were sintered at 1473 K. XRD pattern of BFT90 revealed a mixed structure of *h*-BT and monoclinic $Ba_2Fe_2O_5$ (*m*-BF). Similar results were reported by Gonzalez-Calbet et al.[31)] From these results, it becomes clear that the crystal structure is changed by the Fe concentration.

The resistivity of BFT100*x* ceramics at room temperature as a function of Fe concentration is shown in **Fig. 2**. With increase in Fe concentration, the resistivity of BFT100*x* ceramics decreases. The low resistivity may originate from the substitution of Ti^{4+} with Fe^{3+}, which increases the oxygen vacancy. The temperature dependence of DC resistivity due to the adiabatic hopping of small polarons follows

$$\rho = A \exp\left(\frac{\Delta E_a}{k_B T}\right), \tag{2}$$

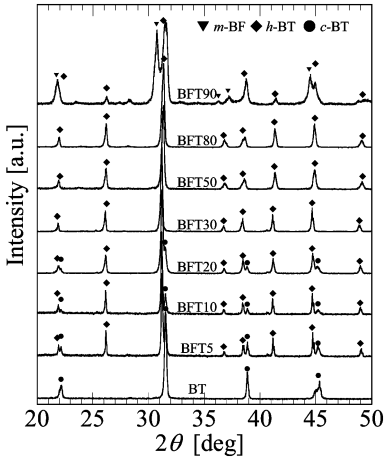

Fig. 1. XRD patterns of BFT100*x* ceramics.

where *A* is a pre-exponential factor, ΔE_a is the activation energy for small polaron hopping, and k_B is the Boltzman constant. We found that the resistivity can be fitted well with Eq. (1) from room temperature to 500 K. **Table 1** lists the resistivity-fitted activation energy ΔE_a in Eq. (1), and the resistivity of BFT100*x* ceramics at 300, 400, and 500 K. Activation energy decreased from 1.07 to 0.43 eV by a 10% Fe substitution, and it further decreased with increase in Fe concentration. This decrease is probably caused by the increase of hopping in the energy states of neighboring polarons at high Fe concentrations.

The Seebeck coefficient and conductivity at 1100 K as a function of Fe concentration is shown in **Fig. 3**. Conductivity of BFT100*x* at 1100 K increased with increase in Fe concentra-

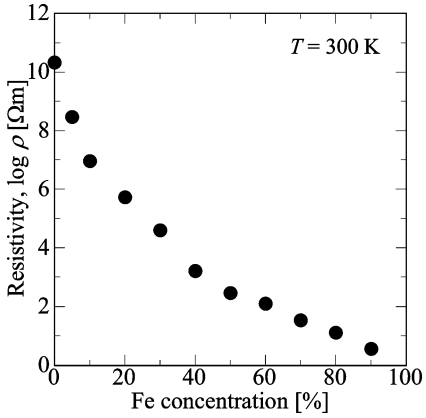

Fig. 2. Resistivity of BFT100*x* ceramics as a function of Fe concentration.

Table 1. Resistivity and activation energy of BFT100*x* ceramics

Fe concentration [%]	Resistivity, ρ [Ωm]			ΔE_a [eV]
	300 K	400 K	500 K	
0	2.1×10^{10}	5.9×10^{9}	3.4×10^{7}	1.07
10	9.2×10^{7}	2.6×10^{5}	1.4×10^{4}	0.43
20	5.3×10^{7}	1.7×10^{4}	1.3×10^{3}	0.37
30	4.0×10^{4}	9.6×10^{2}	8.4×10^{1}	0.40
50	2.9×10^{2}	2.1×10^{1}	2.6×10^{0}	0.35
60	1.3×10^{2}	4.5×10^{0}	6.5×10^{-1}	0.32
70	3.5×10^{1}	1.6×10^{0}	2.7×10^{-1}	0.32
80	1.3×10^{1}	8.3×10^{-1}	1.5×10^{-1}	0.29
90	3.7×10^{0}	3.5×10^{-1}	9.4×10^{-2}	0.23

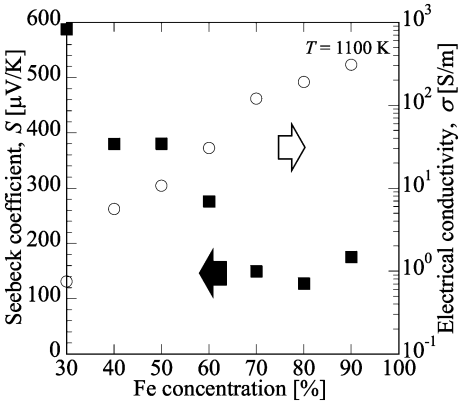

Fig. 3. Seebeck coefficient (solid squares) and conductivity (hollow circles) of BFT100*x* ceramics as a function of Fe concentration at 1100 K.

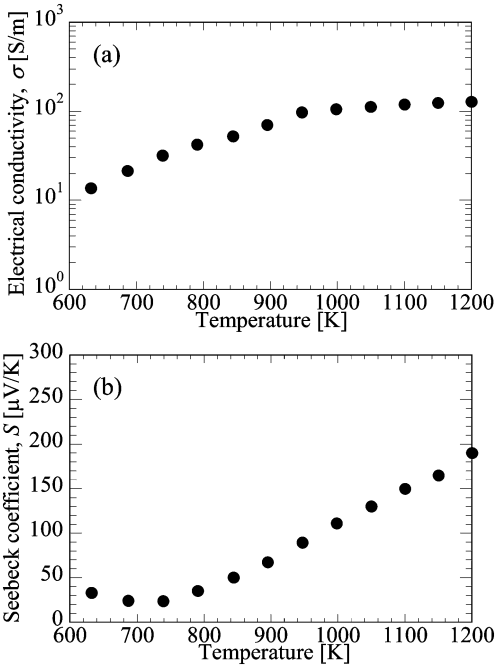

Fig. 4. Temperature dependence of conductivity (a) and Seebeck coefficient (b) for BFT70 ceramics.

tion. BFT90 showed the highest conductivity of 3.1×10^2 S/m at 1100 K. Conversely, the Seebeck coefficient of BFT100x decreased with increase in Fe concentration for $x = 0.40$–0.80; Seebeck coefficient of BFT90 was larger than that of BFT80. The increase of σ and decrease of S suggested an increase in the carrier concentration, which can be attributed to the substitution of Ti^{4+} with Fe^{3+} in the system. The high Seebeck coefficient of BFT90 may be attributable to its crystal structure. Crystal structure of BFT100x was a single phase h-BT structure at $0.40 < x < 0.80$, but that of BFT90 was a mixed structure of h-BT and m-BF. From these results, it seems that m-BF phases of BFT90 have higher Seebeck coefficient than h-BT phase of BFT90. Therefore it is considered that BFT90 with mixed structure of h-BT and m-BF showed the higher Seebeck coefficient than BFT80. The effectiveness of mixed structure increasing high conductivity and Seebeck coefficient was confirmed in $SrFeO_3$–$CaFeO_3$.[32]

The temperature dependence of conductivity (a) and the Seebeck coefficient (b) for BFT70 are shown in **Fig. 4**. The sign of the Seebeck coefficient is positive and therefore the majority of carriers are holes. The Seebeck coefficient and conductivity for all samples increased with increase in the measuring temperature and reached the highest value at 1100–1200 K. The conductivity of all samples was almost saturated at high temperature. The increase in conductivity can be attributed to the increase in carrier concentration, however the increase in Seebeck coefficient cannot be attributed to them. Similar results were reported for $SrFeO_{3-\delta}$,[30] $BaFeO_{3-\delta}$,[30] and $Ca_{3-x}Na_xCo_4O_9$.[33] Honbo et al. considered that the increase in the Seebeck coefficient is also based on the formation of an oxygen vacancy.[30] It appears that the Seebeck coefficient increases due to an increase in oxygen vacancy at high temperatures.

The power factor of BFT100x ceramics as a function of Fe concentration is shown in **Fig. 5**. The conductivity and Seebeck coefficient data in Fig. 3 show that Fe substitution was effective in improving the power factor ($S^2\sigma$) of the $BaFe_xTi_{1-x}O_{3-\delta}$ system. The power factor of BFT100x increased with increase in Fe concentration and increase in temperature from 600 to 1200 K. The power factor of BFT90 reached 9.6 μW/K^2 m around 1100 K, which is three times larger than that of BFT80. The large power factor of BFT90 was due to the coexistence of a large Seebeck coefficient and conductivity at high temperatures. These results suggest that $BaFe_xTi_{1-x}O_{3-\delta}$ ceramics have good potential for application as a high-temperature thermoelectric material.

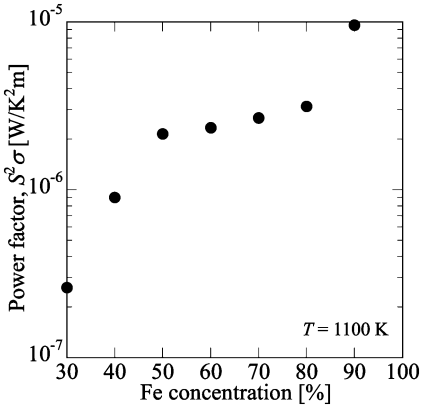

Fig. 5. Power factor of BFT100x ceramics as a function of Fe concentration.

4. Conclusion

In this study, we investigated high-temperature thermoelectric properties of $BaFe_xTi_{1-x}O_{3-\delta}$. The crystal structure of BFT100x was found to be a mixed structure of c-BT and h-BT for $0.05 < x < 0.20$, and a single phase of h-BT for $0.30 < x < 0.80$. XRD pattern of BFT90 showed a mixed structure of h-BT and m-BF. Room temperature resistivity decreased with increase in Fe concentration; this decrease may originate from the substitution of Ti^{4+} with Fe^{3+}, which increases hole concentration. Conductivity increased with increase in Fe concentration and increase in temperature from 600 to 1200 K. Conversely, Seebeck coefficient decreased with increase in Fe concentration and increased with increase in temperature. These results can be attributed to the oxygen defect of BFT100x at high temperatures. BFT90 exhibited a larger Seebeck coefficient than BFT80, which can be attributed to the mixed structure of BFT90. Power factor of BFT90 reached 9.6 μW/K^2 m. These results suggest that there exists a good potential for enhancing the thermoelectric properties of $BaFe_xTi_{1-x}O_{3-\delta}$ ceramics.

Acknowledgments This work was supported in part by a grant from the Institute of Ceramics Research and Education, NITech.

References

1) M. Ohtaki, *J. Ceram. Soc. Japan*, **119**, 770–775 (2011).
2) H. J. Goldsmid, *Proc. Phys. Soc. Lond.*, **71**, 633–646 (1958).
3) K. Hasezaki, Y. Morisaki, H. Araki, H. Kitagawa and E. Tanabe, *Mater. Trans.*, **47**, 383–387 (2006).
4) T. Caillat, M. Carle, P. Pierrat, H. Scherrer and S. Scherrer, *J. Phys. Chem. Solids*, **53**, 1121–1129 (1992).
5) B. Houston, R. E. Strakna and H. S. Belson, *J. Appl. Phys.*, **39**, 3913–3917 (1968).
6) D. M. Powe and V. S. Shukla, *J. Appl. Phys.*, **52**, 7421–7426 (1981).
7) M. Otake, K. Sato, O. Sugiyama and S. Kaneko, *J. Ceram. Soc. Japan*, **111**, 436–438 (2003).

8) M. Otake, K. Sato, O. Sugiyama and S. Kaneko, *J. Ceram. Soc. Japan*, 112, 464–466 (2004).
9) M. Otake, K. Sato, O. Sugiyama and S. Kaneko, *J. Ceram. Soc. Japan*, 111, 907–911 (2003).
10) J.-G. Kim, Y.-Y. Choi, D.-J. Choi, J.-I. Kim, B.-S. Kim and S.-M. Choi, *J. Ceram. Soc. Japan*, 117, 574–577 (2009).
11) C.-H. Pai, *J. Ceram. Soc. Japan*, 112, 88–94 (2004).
12) I. Terasaki, Y. Sasago and K. Uchinokura, *Phys. Rev. B*, 56, R12685–R12687 (1997).
13) I. Matsubara, Y. Zhou, T. Takeuchi, R. Funahashi, M. Shikano, N. Murayama, W. Shin and N. Izu, *J. Ceram. Soc. Japan*, 111, 238–241 (2003).
14) S. Ohta, T. Nomura, H. Ohta and K. Koumoto, *J. Appl. Phys.*, 97, 034106–034109 (2005).
15) T. Okuda, K. Nakanishi, S. Miyasaka and Y. Tokura, *Phys. Rev. B*, 63, 113104–113107 (2001).
16) S. Ohta, H. Ohta and K. Koumoto, *J. Ceram. Soc. Japan*, 114, 102–105 (2006).
17) W. Shin and N. Murayama, *Jpn. J. Appl. Phys.*, 38, 1336–1338 (1999).
18) D. H. Flahaut, R. Funahashi, K. Lee, H. Ohta and K. Koumoto, International Conference on Thermoelectrics, ICT, Proceedings, 103–106 (2006).
19) P.-X. Thao, T. Tsuji and Y. Yamamura, *J. Ceram. Soc. Japan*, 112, S663–S667 (2003).
20) S. Li, R. Funahashi, I. Matsubara, K. Ueno, S. Sodeoka and H. Yamada, *Chem. Mater.*, 12, 2424–2427 (2000).
21) Q.-S. Yu, L. Wang, L. Yu, L.-G. Hua, W.-Y. Qiang and C. Nan, *Trans. Nonferrous Met. Soc. China*, 20, 1911–1915 (2010).
22) I. E. Gery, C. Li, L. M. D. Cranswick, R. S. Roth and T. A. Vanderath, *J. Solid State Chem.*, 135, 312–321 (1998).
23) T. A. Vanderath, J. M. Loezos and R. S. Roth, *J. Solid State Chem.*, 121, 38–50 (1996).
24) R. Mater and J. L. Cohn, *J. Appl. Phys.*, 92, 5429–5436 (2002).
25) R. Mater, J. L. Cohn, J. J. Neumeier and L. A. Bendersky, *Appl. Phys. Lett.*, 78, 2536–2538 (2001).
26) S. Ray, P. Mahadevan, S. Mandal, S. R. Krishnakumar, C. S. Kuroda, T. Sasaki, T. Taniyama and M. Itoh, *Phys. Rev. B*, 77, 104416–104421 (2008).
27) D. Xue, H. Zhang, Y. Li, Y. Lin and Z. Li, *J. Mater. Sci.: Mater. Electron.*, 23, 1306–1312 (2012).
28) X.-K. Wei, Q.-H. Zhang, F.-Y. Li, C.-Q. Jin and R.-C. Yu, *J. Alloys and Comp.*, 508, 486–493 (2010).
29) N. Maso, H. Beltran, E. Cordoncillo, P. Escribano and A. R. West, *J. Mater. Chem.*, 16, 1626–1633 (2006).
30) J. Honbo, Y. Matsumoto and T. Kawano, *J. Solid State Chem.*, 84, 138–143 (1990).
31) J. M. Gonzarez-Calbet, M. Parras, M. Vallet-Regi and J. C. Grenier, *J. Solid State Chem.*, 86, 149–159 (1990).
32) T. Nakamura, Published Japan Patent Application, P2006-108598A [in Japanese].
33) G. Xu, R. Funahashi, M. Shikano, Q. Pu and B. Liu, *Solid State Commun.*, 124, 73–76 (2002).